Kirkendall effect in the two-dimensional lattice-gas model

Vladimir P. Zhdanov*
Department of Physics, Chalmers University of Technology, Göteborg, Sweden
and Boreskov Institute of Catalysis, Russian Academy of Sciences, Novosibirsk, Russia

(Received 7 October 2018; published 17 January 2019)

Customarily, the Kirkendall effect is associated with the vacancy-mediated balance of diffusion fluxes of atoms at the interface between two metals. Nowadays, this effect attracts appreciable attention due to its crucial role in the formation of various hollow nanoparticles via oxidation of metal nanocrystallites. The understanding of the physics behind this effect in general and especially in the case of nanoparticles is still incomplete due to abundant complicating factors. Herein, the Kirkendall effect is illustrated in detail at the generic level by performing two-dimensional (2D) lattice Monte Carlo simulations of diffusion of A and B monomers with attractive nearest-neighbor interaction for times up to 10^7 Monte Carlo steps. Initially, A monomers are considered to form a close-packed array, while B monomers are in the 2D-gas state. The A-B interaction is assumed to be stronger compared to the other interactions, so that thermodynamically the c(2 × 2) A-B phase is preferable compared to the close-packed A phase (as in the case of metal oxidation). Depending on the relative rate of the diffusion jumps of A and B monomers, the patterns observed at the late stage of the formation of the mixed phase are shown to range from a single array without voids to those with appreciable disintegration of the initial array. In this way, the model predicts a single array with numerous small voids, a few moderate voids, or a single large void inside.

DOI: 10.1103/PhysRevE.99.012132

I. INTRODUCTION

The diffusion fluxes of two metals during their contact and formation of an alloy layer at the contact interface can be different. This difference is compensated by diffusion of vacancies and accompanied by the formation of voids in one of the metals near the newly formed metal-alloy interface. These features of diffusion were first observed by Kirkendall in the 1940s [1,2] and since then have been associated with his name (as reviewed in Ref. [3]). In metallurgy, the formation of voids is undesirable, and from this perspective the Kirkendall effect is considered to be negative. During the past decade, this effect was found to be behind the formation of various hollow nanoparticles, e.g., during oxidation of metal nanocrystallites or deposition of one metal on nanoparticles composed of another metal (see the seminal study by Alivisatos *et al.* [4], reviews [5–7], recent experiments [8–11], and references therein). Such nanoparticles are of high current interest in the context of catalysis, photochemistry, nanosensors, and drug delivery. The corresponding experimental studies are numerous, and accordingly the Kirkendall effect is now often associated with hollow nanoparticles and viewed positively from the latter perspective.

The full-scale interpretation of the formation of voids via the Kirkendall pathway is far from straightforward irrespective of whether the process occurs during contact of macroscopic samples or in nanoparticles. For example, the diffusion of metal or oxygen ions via the oxide layer during oxidation of metal nanoparticles is influenced by (i) the electric field generated due to the charge located at the interfaces, (ii) lattice strain arising due to the lattice expansion during the oxide formation, (iii) evolution of the oxide structure, e.g., via the grain growth, and (iv) generation of cracks in the oxide (see, e.g., Refs. [12–16] and references therein). The role of all these factors is often appreciable, and the understanding of their interplay is still incomplete.

One of the ways to clarify complex phenomena is to construct and analyze generic models by focusing on some of the corresponding ingredients and ignoring other ingredients. This approach is widely employed in physics in general and statistical physics in particular. For example, the generic statistical models (e.g., the Ising and lattice gas models models focused on phase transitions [17], various kinetic models of epitaxial growth [18], or Ziff-Gullari-Barshad (ZGB) model of kinetic phase transitions in catalytic reactions [19]) are highly simplified and despite or due to this feature are instructive and form a firm conceptual basis for the understanding of very different phenomena. From this perspective, it seems to be reasonable to identify the simplest statistical model predicting the Kirkendall effect. Following this line, I present and analyze here a simple two-component two-dimensional (2D) lattice-gas model exhibiting features which are reminiscent of those observed during oxidation of metal nanocrystallites. Basically, I illustrate the Kirkendall effect in the 2D lattice gas by using Monte Carlo (MC) simulations. In fact, the simulations presented show that this effect can be reproduced without various complications which are inherent for oxidation of metal nanocrystallites. Thus, the complicating factors, despite their importance, are not crucial for the observation of the Kirkendall effect. In a more general context, the patterns predicted by the model are more complex than one might

*zhdanov@chalmers.se

expect, and this finding validates the report of the results obtained.

II. MODEL

The analysis is focused on diffusion of A and B monomers on a square $L \times L$ lattice. This process is considered to occur via activated jumps of monomers to nearest-neighbor (nn) vacant sites. In the framework of the transition state theory, the corresponding jump rate constants are determined by the preexponential factors, and the activation energy is identified as usual with the difference of the monomer energies in the activated state, i.e., at the saddle points of the potential barriers, and in the ground state, i.e., near the bottom of potential wells [20]. A monomer performing a jump interacts laterally with neighbors, which are in the ground state. Depending on the location of a jumping monomer, there are lateral interactions in the ground and activated states, $\epsilon_{X,i}$ and $\epsilon^*_{X,i}$, where X characterizes the monomer type (X $\equiv$ A or B) and i characterizes the arrangement of neighbors. The difference of these energies determines the contribution of lateral interactions to the jump activation energy. In particular, the rate constant of a jump in one direction is represented as (see Eq. (7.3.15) in Ref. [20])

$$k_{X,i} = k^\circ_X \exp[-(\epsilon^*_{X,i} - \epsilon_{X,i})/k_B T], \tag{1}$$

where k°_X is the corresponding jump rate in the absence of neighbors. In real systems, the lateral interaction in the activated state is often weaker compared to that in the ground state, and accordingly I neglect the former interaction, i.e., set $\epsilon^*_i = 0$. The latter interaction is represented as a sum of the attractive pairwise nn interactions, $\epsilon_{AA} < 0$, $\epsilon_{BB} < 0$, and $\epsilon_{AB} < 0$. In particular, the interaction $\epsilon_{A,i}$ is identified with $n\epsilon_{AA} + m\epsilon_{AB}$, where n and m are the numbers of nn A and B monomers for a jumping A monomer with a given arrangement in the adjacent sites. By analogy, the interaction $\epsilon_{B,i}$ is identified with $n\epsilon_{BB} + m\epsilon_{AB}$, where n and m are the numbers of nn B and A monomers for a jumping B monomer. With this specification, expression (1) is reduced to

$$\begin{aligned} k_{A,i} &= k^\circ_A \exp[(n\epsilon_{AA} + m\epsilon_{AB})/k_B T], \\ k_{B,i} &= k^\circ_B \exp[(n\epsilon_{BB} + m\epsilon_{AB})/k_B T], \end{aligned} \tag{2}$$

where n and n are the numbers corresponding to a jumping A or B monomer and given i.

To perform MC simulations, one needs dimensionless probabilities ($p_i \leqslant 1$) of possible events. To get such probabilities, the rate constants are usually normalized to a suitably chosen rate constant which is larger than or equal to the rate constants of all the possible events. After such normalization, expressions (2) for monomers with attractive nn interactions can be replaced by

$$\begin{aligned} p_{A,i} &= p^\circ_A \exp[(n\epsilon_{AA} + m\epsilon_{AB})/k_B T], \\ p_{B,i} &= p^\circ_B \exp[(n\epsilon_{BB} + m\epsilon_{AB})/k_B T], \end{aligned} \tag{3}$$

where $p^\circ_A \leqslant 1$ and $p^\circ_B \leqslant 1$ are the jump probabilities in the absence of neighbors.

Expressions (1)–(3) based on the transition state theory satisfy the detailed balance principle at the level of single jumps back and forth. This principle can be satisfied by

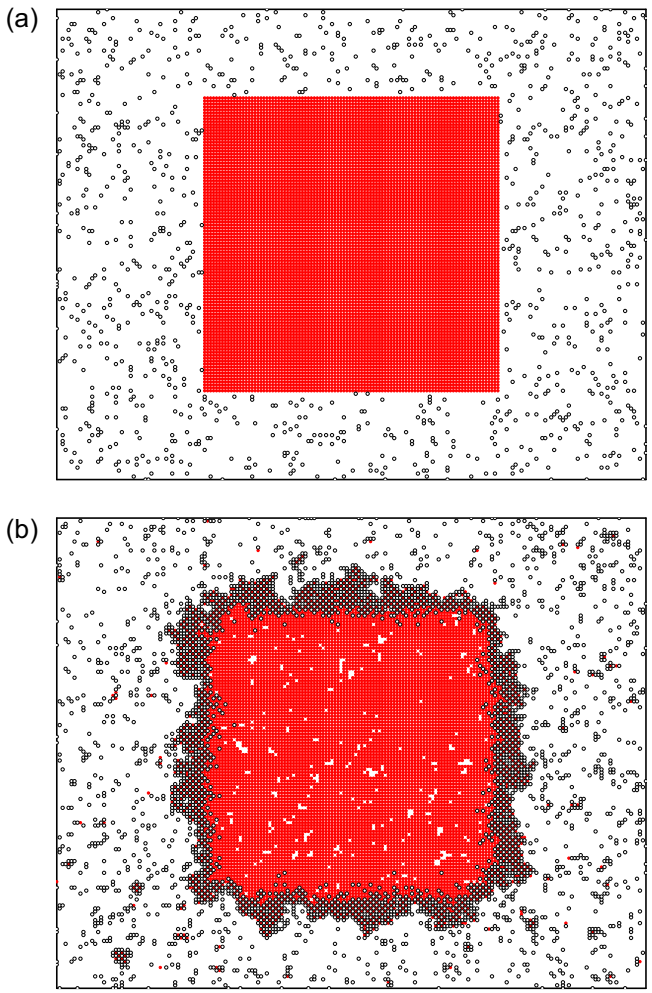

FIG. 1. Snapshots of the central 200×160 strip of the 200×200 lattice during conversion of the A (1×1) phase (with $l = 100$) into the A-B c(2×2) phase with $p^\circ_A = p^\circ_B = 1$ at $t = 0$ (a) and 10^7 MCS (b). Initially, the A $l \times l$ array is located in the center of the lattice. A and B monomers are shown by filled and open circles respectively.

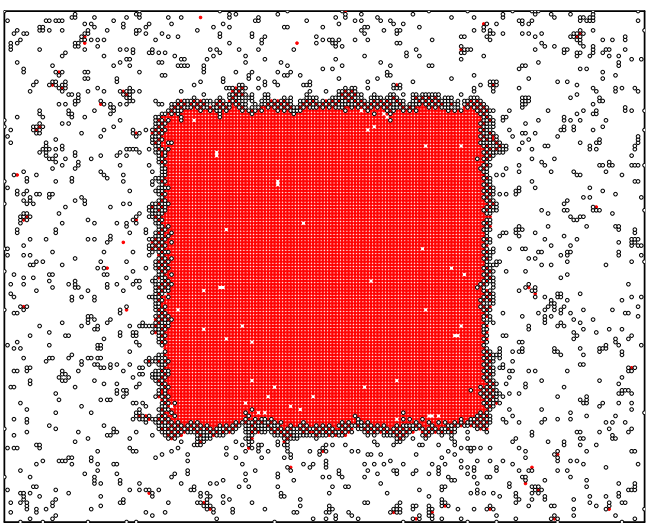

FIG. 2. As in Fig. 1(b) but for $p^\circ_A = 0.1$ and $p^\circ_B = 1$.

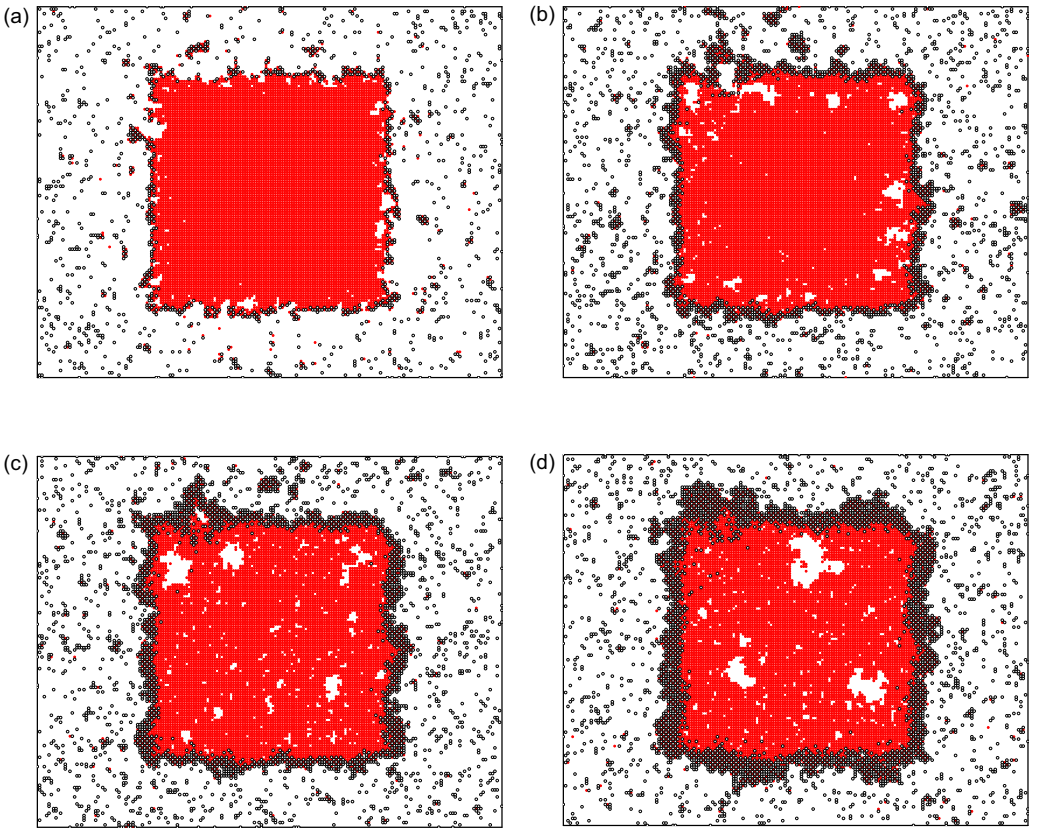

FIG. 3. Snapshots of the central 200 × 160 strip of the 200 × 200 lattice during conversion of the A (1 × 1) phase (with $l = 100$) into the A-B c(2 × 2) phase with $p_A^\circ = 1$ and $p_B^\circ = 0.3$ at $t = 10^4$ (a), 10^5 (b), 10^6 (c), and 10^7 MCS (d). Initially, the A $l \times l$ array is located in the center of the lattice. A and B monomers are shown by filled and open circles respectively.

other choices of the monomer-monomer interactions and/or expressions for the jump rates [21] (the corresponding literature is extensive and can be tracked over several decades; see, e.g., Refs. [22–24]). One of the options is, e.g., to use the conventional Metropolis dynamics. The latter dynamics is faster compared to that defined by (3). It predicts, however, equal rates of jumps of monomer in the dilute phase and holes in the dense phase. In reality, the former jumps are usually much faster. This is also the case according to expressions (1)–(3). From this perspective, the dynamics defined by (3) is preferable.

To mimic oxidation of metal nanocrystallites, I consider that initially (at $t = 0$) A monomers form a close-packed square $l \times l$ array located in the center of the $L \times L$ lattice [like a metal nanocrystallite in the 3D space; see Fig. 1(a)]. The A-A interaction energy, $\epsilon_{AA} = -2k_BT$, is chosen to be sufficiently strong for phase separation with formation of the A (1 × 1) islands in the absence of B monomers (the corresponding critical temperature is well known to be given in this case by $T_{cr} = 0.567|\epsilon_{AA}|$).

B monomers are initially considered to be distributed at random on the sites not occupied by A monomers, and their coverage of these sites is low, $\theta_B^\circ = 0.05$. The B-B interaction energy, $\epsilon_{BB} = -k_BT$, is set to be relatively weak so that these monomers alone are in the one-phase state (i.e., $T > T_{cr} = 0.567|\epsilon_{BB}|$).

The A-B interaction energy, $\epsilon_{AB} = -3k_BT$, is chosen to be stronger than the A-A interaction, so that in the A-B mixture the formation of the A-B c(2 × 2) phase is preferable compared to the A (1 × 1) phase.

On the lattice boundary, I use the no-flux boundary condition, i.e., the jumps of monomers out of the lattice are not allowed. For A monomers, this condition is employed literally. For B monomers, this condition is used in combination with an additional condition taking into account that the initial population of B monomers is not sufficient in order to fully convert the A (1 × 1) phase into the A-B c(2 × 2) phase, and accordingly additional B monomers are needed for this conversion. In oxidation of metal nanocrystallites, the situation is similar in the sense that the amount of oxygen located in the gas phase near a nanocrystallite is not sufficient for its full oxidation, and additional oxygen is supplied from the space far from a nanocrystallite. To mimic such a supply, I employ for B monomers the grand canonical distribution with the initial coverage $\theta_B^\circ = 0.05$ on the border sites during trials of B jumps from the boundary sites to the interior of the lattice.

III. ALGORITHM OF SIMULATIONS

With the specification above, the algorithm of the MC simulations is as follows:

(i) A site is chosen at random.

(ii) If the site chosen is located inside the lattice and vacant, a trial ends.

(iii) If the site chosen is located inside the lattice and occupied, a monomer located in this site tries to diffuse. In

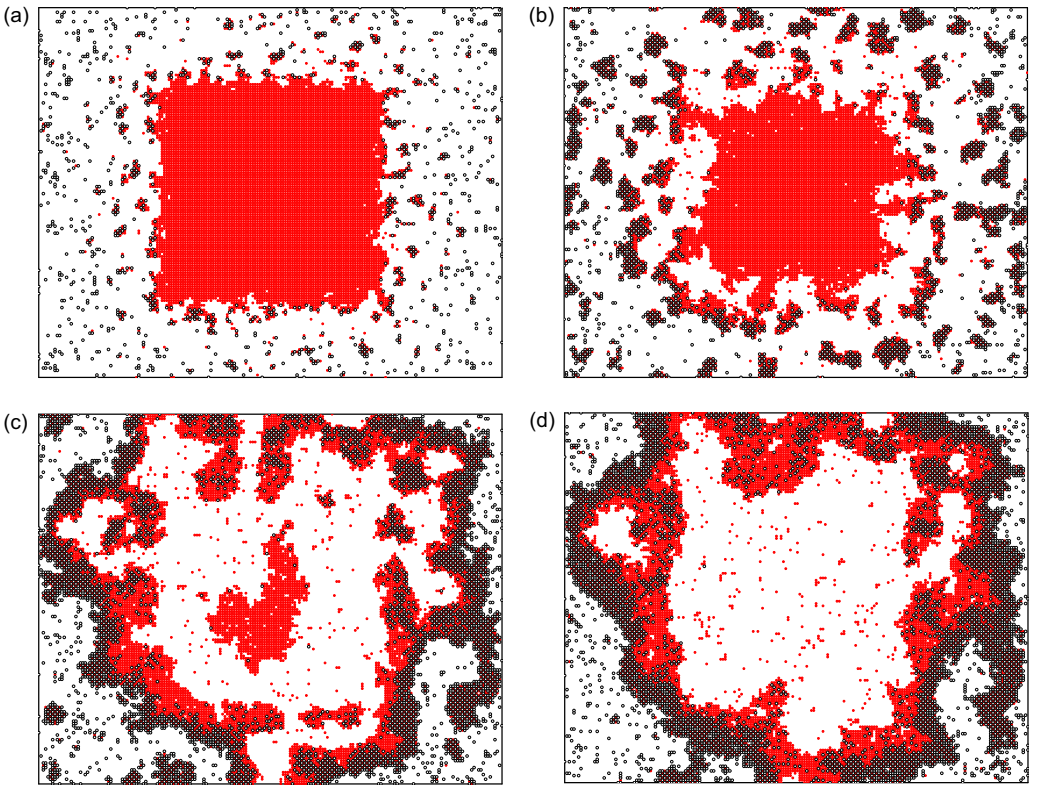

FIG. 4. Snapshots of the central 200 × 160 strip of the 200 × 200 lattice during conversion of the A (1 × 1) phase (with $l = 100$) into the A-B c(2 × 2) phase with $p_A^\circ = 1$ and $p_B^\circ = 0.1$ at $t = 10^4$ (a), 10^5 (b), 10^6 (c), and 10^7 MCS (d). Initially, the A $l \times l$ array is located in the center of the lattice. A and B monomers are shown by filled and open circles respectively.

particular, a nn site is randomly selected, and if the latter site is vacant, the monomer jumps to it with probability $p_{A,i}$ or $p_{B,i}$ [Eq. (3)].

(iv) If the site chosen is located on the boundary and occupied by A, a nn site is randomly selected, and if this site is vacant, the monomer jumps to it with probability $p_{A,i}$.

(v) If the site chosen is located on the boundary and not occupied by A, a random number, $0 < \rho \leqslant 1$, is generated, and the site is considered to be vacant provided $\rho > \theta_B^\circ$ or occupied by B provided $\rho \leqslant \theta_B^\circ$. In the former case, a trial ends. In the latter case, a nn site is randomly selected, and if this site is vacant, the monomer jumps to it with probability $p_{B,i}$. (Taken together, these steps mimic the grand canonical distribution of B monomers at the border sites.)

(vi) After each MC trial, the dimensionless time is incremented by $\Delta t = |\ln(\rho)|/L^2$, where $0 < \rho \leqslant 1$ is a random number.

On average, $\Delta t = 1$ corresponds to L^2 MC trials. In the present simulations, as usual, $\Delta t = 1$ is identified with one MC step (MCS). To convert t into real time, it should be divided by the rate constant which was used for normalization of the jump rate constants. For my goals, the time units are not important, and the time is below represented in MCS.

MC runs were performed on a lattice with $L = 200$ up to $t = 10^7$ MCS. The size of the array of A monomers at $t = 0$ was $l = 100$ or 50.

IV. RESULTS OF SIMULATIONS

Except for the lattice and A-array sizes (L and l), the model under consideration includes six parameters: ϵ_{AA}, ϵ_{BB}, ϵ_{AB}, θ_B°, p_A°, and p_B°. For the bulk of simulations shown in Figs. 1–4, the values of four of them were fixed as already indicated above ($\epsilon_{AA} = -2k_BT$, $\epsilon_{BB} = -k_BT$, $\epsilon_{AB} = -3k_BT$, and $\theta_B^\circ = 0.05$), while the sizes were chosen to be $L = 200$ and $l = 100$. With this specification, there are two remaining parameters, p_A° and p_B°, which where varied in order to illustrate qualitatively different patterns predicted by the model.

By definition, p_A° and p_B° represent the jump probabilities in the absence of neighbors or, in other words, the maximum jump probabilities. If these probabilities are equal, $p_A^\circ = p_B^\circ = 1$, the conversion of the A (1 × 1) phase into the A-B c(2 × 2) phase is accompanied by the formation of vacancies and numerous tiny voids in the former phase [Fig. 1(b)]. One can notice that the interfaces between the c(2 × 2) and (1 × 1) phases and between the c(2 × 2) and 2D-gas phases are rather rough or, in other words, poorly ordered because the temperature is only slightly above the critical ones. If at the level of these probabilities the A jumps are slower, $p_A^\circ = 0.1$ and $p_B^\circ = 1$, the situation is qualitatively similar although single vacancies dominate (Fig. 2). Quantitatively, one can see that the thickness of the c(2 × 2) area is in this case appreciably thinner and accordingly the interfaces between the different phases are more ordered.

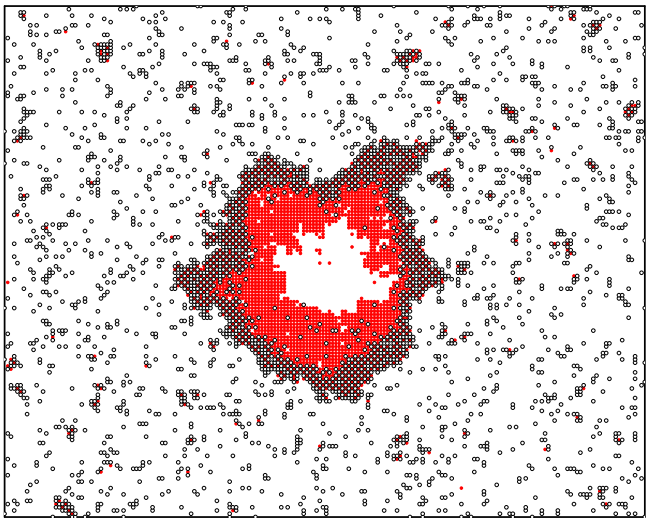

FIG. 5. As in Fig. 3(d) but for $l = 50$.

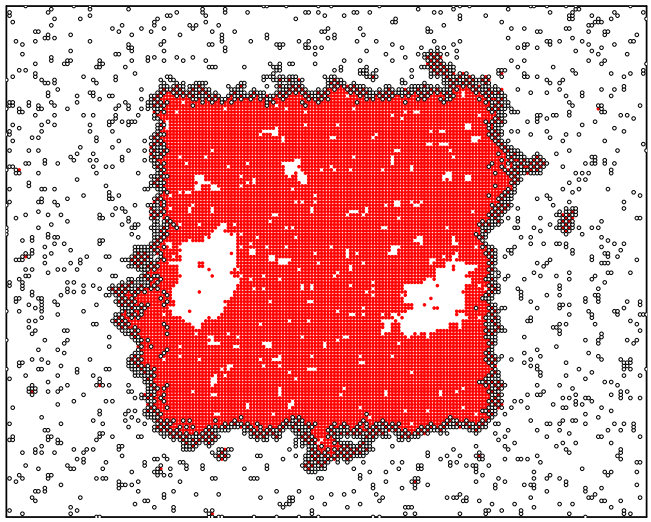

FIG. 7. As in Fig. 3(d) but for $\epsilon_{AB} = -4k_BT$.

If at the level of maximum jump probabilities the B jumps are slower, e.g., $p_A^\circ = 1$ and $p_B^\circ = 0.3$, the conversion of the A (1×1) phase into the A-B c(2×2) phase occurs with the formation of numerous tiny voids and a few voids of appreciable size (Fig. 3). First, the voids are located close to the interface between the c(2×2) and (1×1) phases [Figs. 3(a) and 3(b)]. With increasing time, the number of large voids decreases while their size increases [Figs. 3(c) and 3(d)] as one could expect bearing in mind the driving force for Ostwald ripening. Taken together, the patterns presented in Fig. 3 clearly illustrate the Kirkendall effect in the 2D lattice-gas model. Compared to what is often observed in metal nanocrystallites during oxidation, this effect is not fully developed because there are a few voids. The patterns with a single large void can be generated either by increasing the duration of MC runs or decreasing the initial size of the A (1×1) array (the latter is shown below in Fig. 5).

With decreasing the maximum jump probabilities of the B jumps, the model predicts disintegration of the initial A (1×1) array into large separate A-B c(2×2) islands as shown in Fig. 4 by using $p_A^\circ = 1$ and $p_B^\circ = 0.1$. The process starts by the formation of tiny c(2×2) islands outside the (1×1) array [Fig. 4(a)]. Then, these islands grow [Fig. 4(b)]. The growth is accompanied by coalescence [Fig. 4(b)]. In the end, one can observe a poorly ordered closed structure with a big void inside. The important point is that this whole evolution of the patterns is also is also directly related to the Kirkendall effect.

Comparing the patterns exhibited in Figs. 3(d) and 4(d), one can wonder whether the former one can become similar to the latter one with increasing time (at $t \gg 10^7$ MCS). The fact that the former pattern [Fig. 3(d)] is qualitatively different compared to those [Figs. 4(a)–4(c)] observed before the latter one [Fig. 4(d)] is against this conjecture. With increasing time, on the other hand, the system tends to be closer to thermodynamic equilibrium which is independent of relative rates of diffusion, and it is in favor of similar patterns. The

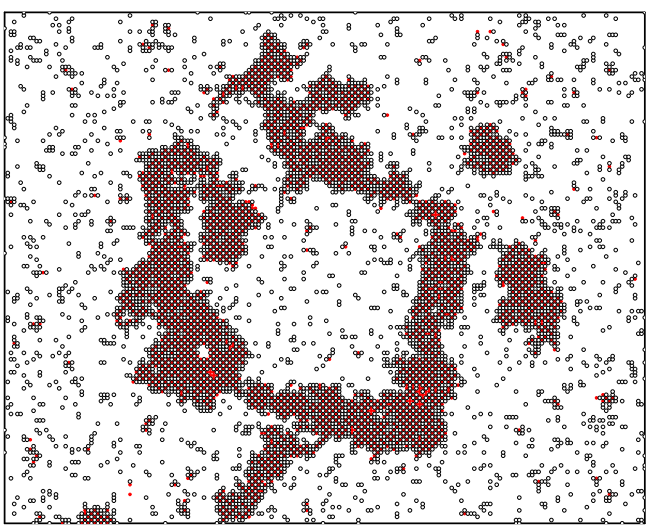

FIG. 6. As in Fig. 4(d) but for $l = 50$.

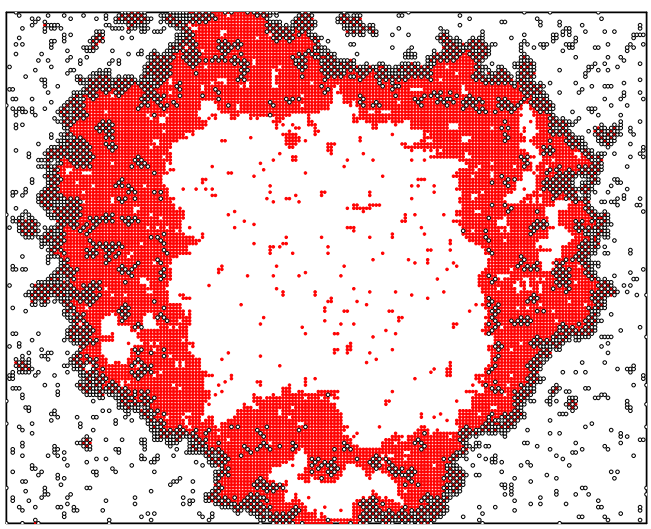

FIG. 8. As in Fig. 4(d) but for $\epsilon_{AB} = -4k_BT$.

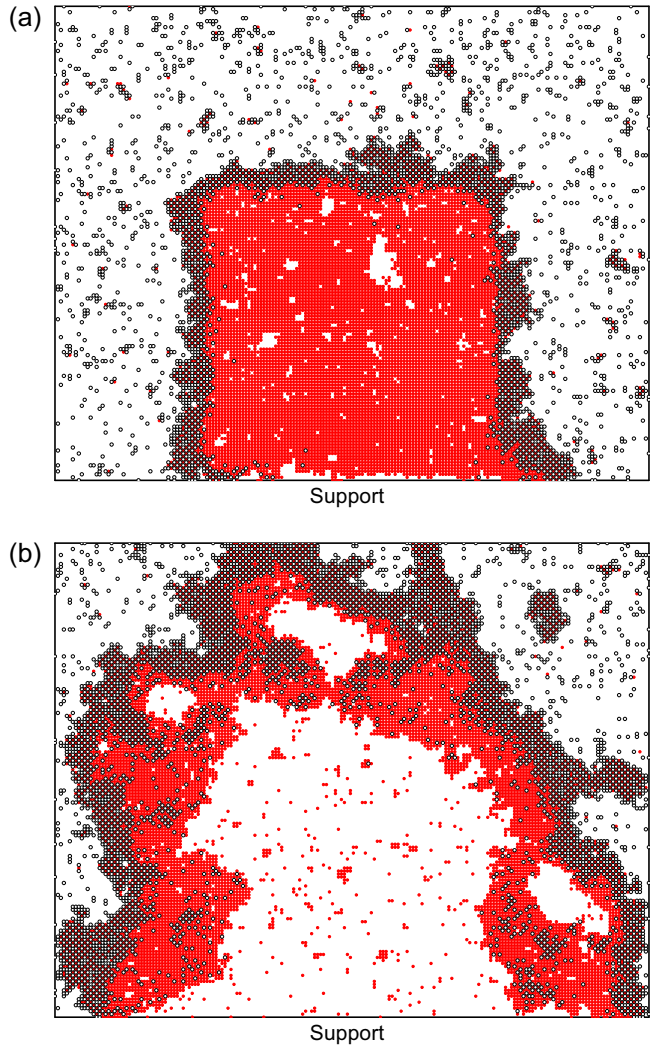

FIG. 9. Snapshots of the lower 200 × 160 part of the 200 × 200 lattice during conversion of the A (1 × 1) phase (with $l = 100$) into the A-B c(2 × 2) phase at $t = 10^7$ with $p_A^\circ = 1$ and $p_B^\circ = 0.3$ (a) and 0.1 (b). Initially, the A $l \times l$ array is located so that one of its sides contacts the lattice boundary. A and B monomers are shown by filled and open circles respectively.

latter argument appears to be stronger. Thus, the response to the question raised is expected to be positive.

The patterns shown in Figs. 3 and 4 were obtained for $p_A^\circ = 1$ and $p_B^\circ = 0.3$ and 0.1. To illustrate in more detail the evolution of patterns with decreasing p_B°, the complementary results for the same value of p_A° and $p_B^\circ = 0.25$, 0.2, 0.15, and 0.05 are presented in the Supplemental Material [25]. Taking together, these patterns show that appreciable changes in the patterns takes place at $p_B^\circ \simeq 0.1$. Although this apparent critical value can easily be identified, the changes can, however, hardly be interpreted in terms of kinetic phase transitions (Refs. [19,26]) because asymptotically (at long MC runs) the system is close to thermodynamic equilibrium.

The snapshots exhibited in Figs. 3 and 4 are especially interesting in the context of the Kirkendall effect, and accordingly it is instructive to show their change with variation of some of the other parameters. Following this line, I first present (Figs. 5 and 6) the results of simulations with the same parameters but for a smaller array (with $l = 50$) of A monomers. In another set of simulations, I kept $l = 100$ but increased the driving force for the formation of A-B c(2 × 2) phase by using $\epsilon_{AB} = -4k_BT$ instead of $-3k_BT$ (Figs. 7 and 8). In both cases, the snapshots are basically similar to those exhibited in Figs. 4 and 5. This means that the features predicted are not too sensitive to variation of l or ϵ_{AB}. There are, however, also some minor qualitative differences. In particular, comparing the snapshots shown in Figs. 3(d) and 5, one can notice that the latter one is more similar to those observed during oxidation of metal nanocrystallites. Comparing the snapshots shown in Figs. 3(d) and 5, one can conclude that the latter one is less interconnected and simultaneously is more converted to the c(2 × 2) state. With increasing monomer-monomer interaction, the snapshots become more compact (cf. Figs. 7 and 8 with Figs. 3 and 4).

In experiments, metal nanocrystallites are usually supported, and accordingly there is no oxygen supply underneath. In the model under consideration, the latter aspect can be mimicked by locating initially the A ($l \times l$) array so that one of its sides contacts one of the lattice boundaries and by canceling item (v) in the MC algorithm for the sites located at this boundary. The corresponding patters (Fig. 9) observed in the end of MC runs with the same parameters as those in Figs. 3 and 4 show that as expected the c(2 × 2) phase is not formed near the boundary. In contrast, the formation of voids is favorable there especially at low value of p_B° [Fig. 9(b)].

V. CONCLUSION

The 2D MC simulations presented illustrate the specifics of the formation of a mixed phase from a spot of a homogeneous phase for times up to 10^7 MCS. MC runs with such duration are usually considered to be long. In the model under consideration, this duration was, however, not always sufficient in order to reach the full conversion to the mixed phase. With this reservation, the results obtained are sufficient in order to clarify what may happen in the framework of the model proposed.

Depending on the relative rate of the diffusion jumps of A and B monomers, the patterns observed at the late stage of the formation the mixed phase are shown to range from a single array without voids to those with appreciable disintegration of the initial array and subsequent partial backward aggregation. In this way, the model predicts a single array with numerous small voids, a few moderate voids, or a single large void inside. Taken together, the patterns presented clearly illustrate the Kirkendall effect in the 2D case. The important point is that these patterns are more complex than one might expect. Basically, this is the main message of this work. There are also other less global novel results, e.g., illustration of the scale of the fluctuations of the array shape and the type of the void distributions.

Although this study was motivated by experiments showing the formation of hollow nanoparticles via oxidation of metal nanocrystallites, the results obtained are obviously of interest also in other contexts. From the perspective of statistical physics, this work illustrates unconventional scenarios of Ostwald ripening. MC simulations of 2D Ostwald

ripening have a long history beginning in the 1980s (see, e.g., Refs. [27–30]). The bulk of such simulations are focused, however, on one-component systems with a random initial distribution (concerning mixed systems, see Ref. [30]).

In the context of surface science, the simulations presented show the above-described nontrivial effects (formation of voids, appreciable disintegration, and partial backward aggregation) which can take place during diffusion of adsorbates with attractive lateral interactions (concerning 2D diffusion, see Refs. [31–34] and references therein). With the current development of surface science such effects can in principle be observed experimentally.

[1] E. O. Kirkendall, Diffusion of zinc in alpha brass, Trans. Am. Inst. Min. Metall. Eng. **147**, 104 (1942).

[2] A. D. Smigelskas and E. O. Kirkendall, Zinc diffusion in alpha-brass, Trans. Am. Inst. Min. Metall. Eng. **171**, 130 (1947).

[3] A. Paul, T. Laurila, V. Vuorinen, and S. V. Divinski, *Thermodynamics, Diffusion and the Kirkendall Effect in Solids* (Springer, Heidelberg, 2014).

[4] Y. Yin, R. M. Rioux, C. K. Erdonmez, S. Hughes, G. A. Somorjai, and A. P. Alivisatos, Formation of hollow nanocrystals through the nanoscale Kirkendall effect, Science **304**, 711 (2004).

[5] H. J. Fan, U. Gösele, and M. Zacharias, Formation of nanotubes and hollow nanoparticles based on Kirkendall and diffusion processes: A review, Small **3**, 1660 (2007).

[6] W. Wang, M. Dahl, and Y. Yin, Hollow nanocrystals through the nanoscale Kirkendall effect, Chem. Mater. **25**, 1179 (2013).

[7] X. Wang, J. Feng, Y. Bai, Q. Zhang, and Y. Yin, Synthesis, properties, and applications of hollow micro-/nanostructures, Chem. Rev. **116**, 10983 (2016).

[8] M. D. Susman, Y. Feldman, T. A. Bendikov, A. Vaskevich, and I. Rubinstein, Real-time plasmon spectroscopy study of the solid-state oxidation and Kirkendall void formation in copper nanoparticles, Nanoscale **9**, 12573 (2017).

[9] N. Pegios *et al.*, Ni nanoparticles and the Kirkendall effect in dry reforming of methane, Appl. Surf. Sci **452**, 239 (2018).

[10] Y. Xiong *et al.*, Tuning surface structure and strain in Pd-Pt core-shell nanocrystals for enhanced electrocatalytic oxygen reduction, Small **13**, 1603423 (2017).

[11] H. Shan *et al.*, Nanoscale kinetics of asymmetrical corrosion in core-shell nanoparticles, Nat. Commun. **9**, 1011 (2018).

[12] V. P. Zhdanov and B. Kasemo, Cabrera-Mott kinetics of oxidation of nm-sized metal particles, Chem. Phys. Lett. **452**, 285 (2008).

[13] A. Ermoline and E. L. Dreizin, Equations for the Cabrera-Mott kinetics of oxidation for spherical nanoparticles, Chem. Phys. Lett. **505**, 47 (2011).

[14] V. P. Zhdanov and B. Kasemo, On the feasibility of strain-induced formation of hollows during hydriding or oxidation of metal nanoparticles, Nano Lett. **9**, 2172 (2009).

[15] L. Klinger and E. Rabkin, On the nucleation of pores during the nanoscale Kirkendall effect, Mater. Lett. **161**, 508 (2015).

[16] V. P. Zhdanov, Oxidation of metal nanoparticles with the grain growth in the oxide, Chem. Phys. Lett. **674**, 136 (2017).

[17] W. H. Weinberg, Order-disorder phase transitions in chemisorbed overlayers, Annu. Rev. Phys. Chem. **34**, 217 (1983).

[18] C. Ratsch, A. Zangwill, P. Smilauer, and D. D. Vvedensky, Saturation and Scaling of Epitaxial Island Densities, Phys. Rev. Lett. **72**, 3194 (1994).

[19] R. M. Ziff, E. Gulari, and Y. Barshad, Kinetic Phase Transitions in an Irreversible Surface-Reaction Model, Phys. Rev. Lett. **56**, 2553 (1986).

[20] V. P. Zhdanov, *Elementary Physicochemical Processes on Solid Surfaces* (Plenum, New York, 1991).

[21] S. J. Manzi, G. A. Ranzuglia, and V. D. Pereyra, One-dimensional diffusion: Validity of various expressions for jump rates, Phys. Rev. E **80**, 062104 (2009).

[22] A. B. Bortz, M. H. Kalos, and J. L. Lebowitz, A new algorithm for Monte Carlo simulation of Ising spin systems, J. Comput. Phys. **17**, 10 (1975).

[23] H. C. Kang and W. H. Weinberg, Dynamic Monte Carlo with a proper energy barrier: Surface diffusion and two-dimensional domain ordering, J. Chem. Phys. **90**, 2824 (1989).

[24] F. M. Bulnes, V. D. Pereyra, and J. L. Riccardo, Collective surface diffusion: n-fold way kinetic Monte Carlo simulation, Phys. Rev. E **58**, 86 (1998).

[25] See Supplemental Material at http://link.aps.org/supplemental/10.1103/PhysRevE.99.012132 for additional lattice snapshots complementing Figs. 3 and 4.

[26] V. P. Zhdanov and B. Kasemo, Kinetic phase transitions in simple reactions on solid surfaces, Surf. Sci. Rep. **20**, 113 (1994).

[27] D. A. Huse, Corrections to late-stage behavior in spinodal decomposition: Lifshitz-Sllyyzov scaling and Monte-Carlo simulations, Phys. Rev. B **34**, 7845 (1986).

[28] V. P. Zhdanov, Island growth and phase separation in chemically reactive adsorbed overlayers, Surf. Sci. **392**, 185 (1997).

[29] S. Puri, A. J. Bray, and J. L. Lebowitz, Phase-separation kinetics in a model with order-parameter-dependent mobility, Phys. Rev. E **56**, 758 (1997).

[30] V. P. Zhdanov, Two-dimensional Ostwald ripening on a patterned support and in a mixed overlayer, Surf. Sci. **644**, 191 (2016).

[31] J. V. Barth, Transport of adsorbates at metal surfaces: From thermal migration to hot precursors, Surf. Sci. Rep. **40**, 75 (2000).

[32] T. Ala-Nissila, R. Ferrando, and S. C. Ying, Collective and single particle diffusion on surfaces, Adv. Phys. **51**, 949 (2002).

[33] J. J. Torrez Herrera, G. A. Ranzuglia, S. J. Manzi, and V. D. Pereyra, Effect of particle-hole symmetry on the behavior of tracer and jump diffusion coefficients, Phys. Rev. E **87**, 052101 (2013).

[34] V. P. Zhdanov, Diffusion of adsorbed particles with attractive lateral interactions at low temperature, Surf. Sci. **617**, 199 (2013).